ELSEVIER

International Journal of Solids and Structures 41 (2004) 3929–3948

INTERNATIONAL JOURNAL OF SOLIDS and STRUCTURES

www.elsevier.com/locate/ijsolstr

Modeling of elastomeric materials using nonlinear fractional derivative and continuously yielding friction elements

Deepak S. Ramrakhyani *, George A. Lesieutre, Edward C. Smith

Department of Aerospace Engineering, Pennsylvania State University, 227 Hammond Building, University Park, PA 16803, USA

Received 2 June 2003; received in revised form 13 February 2004
Available online 19 March 2004

Abstract

A model of the one-dimensional dynamic behavior of elastomeric materials is developed based on a previously existing model. An initial model consisted of nonlinear multiple anelastic displacement fields in parallel with discrete friction elements. The motivation for the development of a new model is reduction of the number of parameters needed to accurately capture material behavior. A new element, a "continuously yielding element," is developed, which conceptually represents a distribution of parallel friction elements. This element replaces the entire collection of discrete friction elements used in the initial model. In addition, a linear fractional derivative anelastic displacement field element replaces the multiple linear anelastic displacement field elements used in the older model. Finally, nonlinearity is introduced into the fractional derivative anelastic displacement field element, in an attempt to capture observed amplitude dependence of storage and loss moduli at higher amplitudes. The different parts of the new model are first compared individually to those of the initial model then combined and compared as an integrated whole. The new model captures the frequency and amplitude variation of the storage and loss moduli of the material better than the initial model, while the total number of parameters is reduced to seven from sixteen.

Keywords: Continuously yielding element; Friction element; Fractional derivative; Elastomer; Time domain; Viscoelasticity

1. Introduction

High-damping elastomeric materials find wide use in engineering applications. For example, they are used in dampers in helicopter rotors, in engine mounts to provide vibration isolation, and for seismic isolation of large structures such as nuclear power plants. The motivation behind this research is the application of such materials to dampers in helicopter rotors. In this case, elastomeric materials, deforming primarily in shear, are used to damp the in-plane vibrations of the rotor to ensure aeromechanical stability.

* Corresponding author. Tel.: +1-814-861-8771; fax: +1-814-865-7092.
E-mail address: deepaksr@psu.edu (D.S. Ramrakhyani).

0020-7683/$ - see front matter © 2004 Elsevier Ltd. All rights reserved.
doi:10.1016/j.ijsolstr.2004.02.034

There are many complex and often unique design issues associated with the design of elastomeric dampers. The stiffness and damping properties of an elastomeric material depend on the frequency and amplitude of excitation and also on the temperature. To facilitate damper design, the nonlinear behavior of the elastomer material needs to be captured accurately in a compact model, preferably one having a minimum number of parameters for a required level of accuracy.

Over the years, various models have been developed, both frequency-domain and time-domain, to capture the behavior of elastomeric materials. For many years, the preferred method of describing the stiffness and damping properties of elastomers was in the frequency domain, using storage and loss moduli, the real and imaginary parts of the complex modulus (Kunz, 1997). This method models the damper as a linear spring and a linear viscous damper operating in parallel. Recent research has focused on time-domain modeling of elastomeric dampers. Panda et al. (1996) developed a nonlinear damper based on the local displacement and local peak strain. The effectiveness of this model over a large range of amplitudes and frequencies has not yet been demonstrated in the literature. A nonlinear viscoelastic solid model was also developed by Gandhi and Chopra (1996). This model uses several nonlinear spring elements combined with a linear dashpot. While the nonlinear spring improves the fidelity of static response, the hysteresis loops are not accurate (Brackbill et al., 2000).

Another approach that has been used to model the dynamic response of elastomers is based on the concept of anelastic displacement fields (ADF). The ADF approach is a physically motivated continuum model originally developed to model the apparent frequency dependent stress–strain behavior of linear viscoelastic materials (Lesieutre et al., 1996; Lesieutre, 1992). In the ADF approach, the total displacement of the material under a load is considered to be the sum of two parts: (1) an elastic part and (2) an anelastic part. The physical interpretation of the single-ADF concept is shown in Fig. 1; the elastic displacement is proportional to the instantaneous load, while the anelastic displacement continuously relaxes to an equilibrium value. The anelastic part itself might consist of several sub-parts. In general, adding more anelastic fields (internal variables) improves the accuracy of this linear viscoelastic model over a broad frequency range.

Continuing research using this approach of multiple anelastic displacement fields by the latter authors has led to the development of a general *nonlinear* time-domain model that captures the dependence of stiffness and damping properties on strain amplitude, frequency, and temperature (Brackbill et al., 2000; Govindswamy et al., 1995). One kind of softening nonlinearity is introduced in the dissipative part of the ADF, by using a nonlinear anelastic stress and anelastic strain-rate relationship. Another, in the form of friction damping and linear spring elements, is added in parallel with the nonlinear ADF model. A friction element is characterized by a yield stress, i.e., a stress beyond which the element yields and the stress across the element remains constant even when the strain increases. Such friction–spring elements are discussed in the literature as a means of capturing the rate-independent nonlinear dissipative behavior of materials (Austrell, 1997). In general, this nonlinear multi-ADF and friction element (NMAF) model can include several internal inelastic fields and several friction–spring pairs. This model is shown schematically in Fig. 2.

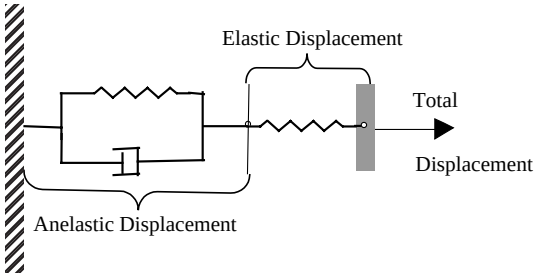

Fig. 1. Physical interpretation of the single-ADF model.

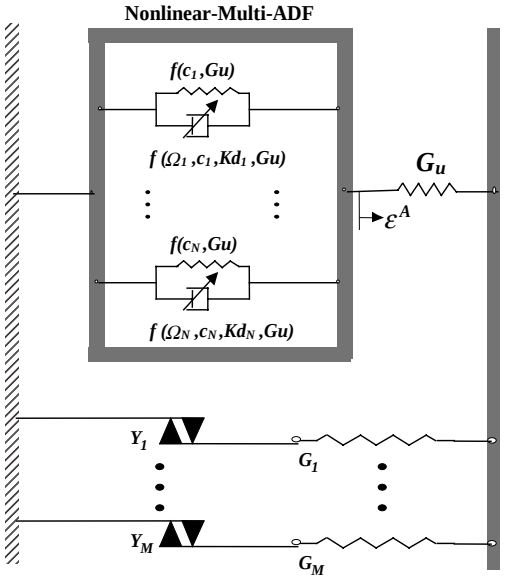

Fig. 2. Mechanism based division of the NMAF model.

The constitutive equations of this model are:

$$\sigma = G_u\varepsilon - G_u\sum_{i=1}^{N}\varepsilon_i^{\mathrm{A}} + \sum_{j=1}^{M}\sigma_j^{\mathrm{f}} \tag{1}$$

$$\frac{c_i G_u}{\Omega_i}\dot{\varepsilon}_i^{\mathrm{A}} = \sigma_i^{\mathrm{A}} + \frac{c_i G_u}{\Omega_i}k_{d_i}(\sigma_i^{\mathrm{A}})^3 \quad (i = 1,\ldots,N) \tag{2}$$

$$\sigma_i^{\mathrm{A}} = G_u(\varepsilon - c_i\varepsilon_i^{\mathrm{A}}) \quad (i = 1,\ldots,N) \tag{3}$$

$$\sigma_j^{\mathrm{f}} = \begin{matrix} G_j\varepsilon & \text{if } \sigma_j^{\mathrm{f}} < Y_j \\ Y_j & \text{if } \sigma_j^{\mathrm{f}} \geqslant Y_j \end{matrix} \quad (j = 1,\ldots,M) \tag{4}$$

Eq. (1) gives the total stress as the sum of stress in the nonlinear-multi-ADF element (first two terms) and the friction–spring pairs (third term). In this equation, σ is the total stress; ε is the total strain; $\varepsilon_i^{\mathrm{A}}$ is the anelastic strain, i.e., the strain in each dashpot of the nonlinear-multi-ADF element; G_u is the high frequency modulus of the nonlinear-multi-ADF element; σ_j^{f} is the stress in each friction–spring pair. Eq. (2) is the relaxation equation relating the anelastic strain rate to the anelastic stress (σ_i^{A}). In this equation c_i relates the stiffness of each of the spring of the ADF element to the high frequency modulus (G_u); K_d is the nonlinear factor of each dashpot; Ω_i is the inverse of relaxation time at constant strain of the dashpot. The relaxation time is the time constant, associated with the decay of the anelastic strain to equilibrium value, when an initial total strain is applied. Eq. (3) gives the anelastic stress in terms of the total strain and the anelastic strain. Eq. (4) gives the stress in each of the friction–spring elements. Here, G_j is the stiffness of the spring, and Y_j is the yield stress of the friction element. Note that when multiple ADF are included, each field requires a set of parameters for K_d, Ω and c; but there is only a single value for G_u. In Eqs. (1)–(4), N anelastic displacement fields and M friction–spring pairs are used. Motivated by helicopter lag damper applications, the NMAF model was validated in the frequency range of quasi-static to 10 Hz and strain

amplitude range of 0.1–20%. Three anelastic displacement fields and three friction–spring pairs were used to match the predictions of this model to experimental data. The model captures the stress response quite accurately over the frequency and amplitude range of interest, but uses 16 parameters to do so, not including additional parameters for temperature dependence. The model can sometimes be cumbersome to characterize and there may be issues of uniqueness. In order to reduce the number of parameters involved, a new model is developed herein, building on the preceding model. The new model uses fractional derivatives and a continuously yielding element.

The models described to this point use integer derivatives to capture dynamic behavior. Fractional derivatives provide an alternate approach. In a series of papers, Bagley and Torvik and Bagley and Calico developed a fractional derivative model of viscoelastic material behavior and applied it to a number of structural modeling and response problems (Bagley and Torvik, 1983, 1985; Bagley and Calico, 1991). An important feature of this approach is its ability to capture the relatively weak frequency dependence of storage and loss moduli exhibited by many materials, using just a few, typically four, model parameters. This feature makes the fractional derivative model especially useful in frequency-domain analysis. Bagley and Torvik initially developed frequency-domain finite elements that could predict structural responses for load histories that have Laplace transforms. In later work, Bagley and Calico (1991) developed a time-domain version with fractional state equations. In the time domain, the presence of fractional operators makes the solution of structural dynamics equations somewhat more complicated than it is for those involving ordinary differential operators.

Enelund and Lesieutre (1998) later introduced fractional derivatives in the anelastic part of a single-ADF model. This model captured the frequency dependence of the loss factor better than the multi-ADF model, and used fewer parameters. Time-domain expressions for the corresponding stress relaxation modulus and the relaxation spectrum were presented.

The objective of the present research is to develop a time domain model that accurately captures the frequency- and amplitude-dependence of elastomer mechanical behavior in a uni-axial stress state (shear), using fewer parameters than the NMAF model. Different parts of the current approach were reported previously by the authors in two conference papers (Ramrakhyani et al., 2001, 2002) but are included here for the sake of completeness. The new model is developed using the NMAF model as a starting point. The NMAF model can be divided conceptually into three parts, the linear multiple ADF elements, the non-linear ADF viscous dashpots, and parallel discrete friction elements as shown in Fig. 3. The main features of the approach used to improve the model include:

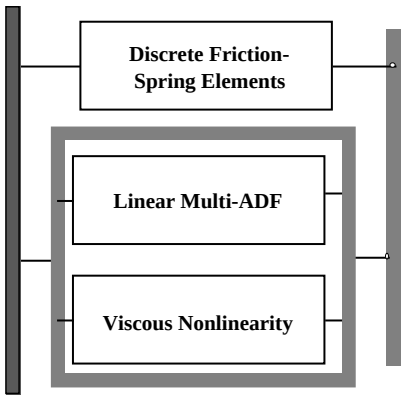

Fig. 3. Conceptual division of the NMAF model.

1. replacing the discrete friction–spring elements with a continuously yielding element;
2. replacing the multiple linear ADF elements with a linear fractional derivative element; and
3. introducing nonlinearity in the fractional derivative element to capture the behavior of elastomers at higher amplitudes better, in a way that is analogous to the nonlinear viscous aspect of the NMAF model.

Each of these elements of the new model is described in a separate section. They are then compared to the corresponding parts of the initial NMAF model. The predictions of the entire model with all three parts are combined compared to experimental data. An added benefit of a more compact model that has fewer parameters is that the parameters take on increased physical significance.

2. Continuous yielding element

In the NMAF model, discrete-spring–friction elements are used to capture rate-independent nonlinearity. Each of these friction elements uses two parameters: the ultimate yield stress, Y_j, and the stiffness, G_j. The spring-friction element can be shown as a linear spring connected in series with a friction element as shown in Fig. 4.

The friction element is locked initially when the strain is 0. As the strain in the element increases, the stress increases linearly, and when the stress in the spring reaches the yield stress of the friction element, the element yields. As the strain continues to increase, the stress in the element remains constant. This occurs for both positive and negative monotonically changing strains. This behavior can be seen in Fig. 5.

The stress–strain behavior of three of these friction–spring elements connected in parallel is shown in Fig. 6. The three friction elements have different yield stresses, Y_1, Y_2, Y_3, and the corresponding springs have stiffnesses G_1, G_2, G_3. As the strain increases from 0, the stresses increase in all three elements. Consider the

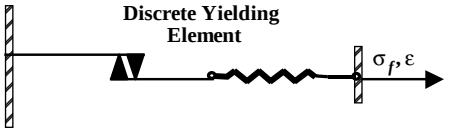

Fig. 4. Spring–friction element.

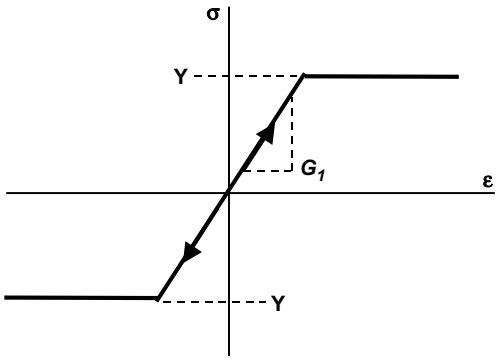

Fig. 5. Behavior of a spring–friction element for increasing or decreasing strain.

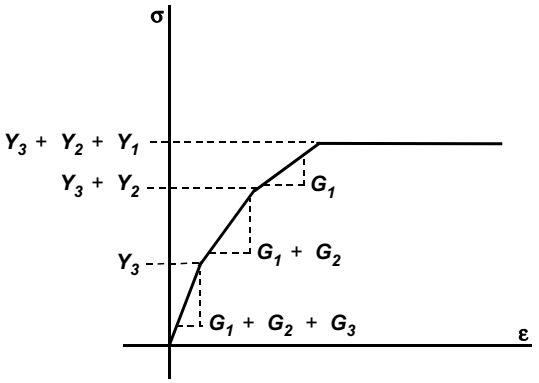

Fig. 6. Behavior of multiple spring–friction elements in parallel.

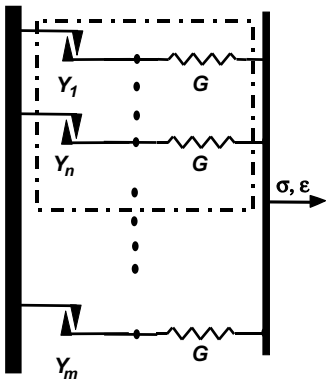

Fig. 7. Schematic of the continuously yielding element.

case when the spring-friction element pair G_3, Y_3, yields first. The total stiffness for increasing strain in this case is due to two springs and is equal to $G_1 + G_2$. When the second element yields, the total stiffness is just G_1, and when the last element yields the stiffness is 0. At this point, the stress can no longer increase and is equal to the ultimate yield stress, which is given by $Y_1 + Y_2 + Y_3$. The continuously yielding element captures the behavior of a large number of such friction–spring elements in parallel, in which the yield stress of each of these friction elements is infinitesimally higher than that of the previous one. As the strain increases the elements yield one by one until all elements have yielded.

Consider a system with m, ($m \to \infty$) friction–spring elements in parallel, as shown in Fig. 7. As the strain is increased, springs $1, 2, 3, \ldots, n$, yield in turn. The fraction of elements yielded can now be defined as shown in Eq. (5).

$$a_y = \frac{\sum_{j=1}^{n} G_j}{\sum_{j=1}^{m} G_j} \tag{5}$$

If all the springs are assumed to have equal stiffness then the fraction of yielded elements, a_y, henceforth called the "yielded area fraction," can be written as:

$$a_y = \frac{n}{m} \tag{6}$$

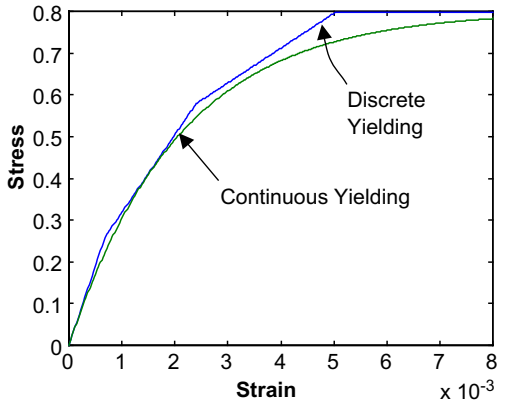

Fig. 8. Stress–strain behavior of both discrete and continuous yielding models for increasing strain.

As the strain increases, the number of elements that yield increases and hence the yielded area fraction increases. Assume that this yielded area fraction, a_y, varies linearly [1] with stress, i.e.,

$$a_y = \mu|\sigma| \tag{7}$$

The current stiffness of the system for increasing strain, k, is due to the contribution of only those elements that have not yielded. This can be expressed in terms of the total stiffness, K, as:

$$k = (1 - a_y)K \tag{8}$$

The incremental stress is related to the incremental strain as follows:

$$d\sigma = k\, d\varepsilon \tag{9}$$

Substituting the value of k, from Eq. (8) and a_y from Eq. (9), and integrating gives:

$$\sigma = \frac{1}{\mu}[1 - e^{-\mu K \varepsilon}] \tag{10}$$

Eq. (10) gives the relationship between the stress and strain of a continuously yielding element, for increasing strain. In this expression, as $\varepsilon \to \infty$ all the elements yield and the corresponding stress is the total yield stress. Thus, the variable μ is the inverse of the total yield stress. The variable K is the initial stiffness when the strain is 0. The stress–strain behavior of the continuously yielding element is compared to that of the three discrete friction–spring elements in Fig. 8, for continuously increasing strain.

If the discrete friction–spring model is expressed in terms of the product of fractional area yielded and initial stiffness, and the variation of the yielded area with increasing stress is plotted, the yielded area is a stepped function, as shown in Fig. 9.

Eq. (10) gives a nonlinear relation between stress and strain for increasing strain. This equation just represents a nonlinear spring; the dissipative behavior of a friction element has not yet been addressed. Fig. 10 shows the behavior of a single friction–spring element under conditions of increasing, then decreasing strain. As the strain is increased, the stress increases linearly until the friction element yields (point 2) and the stiffness becomes 0 and the strain increases to point 3. Then, the strain is decreased until the friction

[1] Note that some other variation could be used instead of the linear variation that is used here.

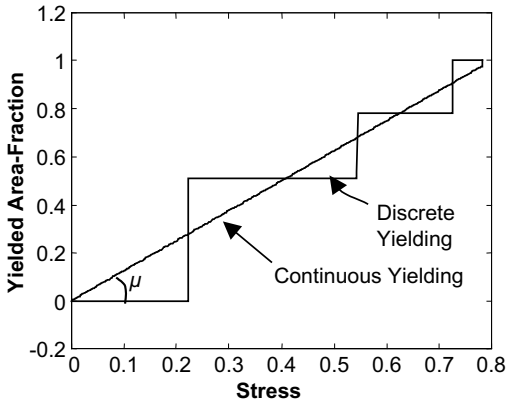

Fig. 9. Comparison of yielded area fraction.

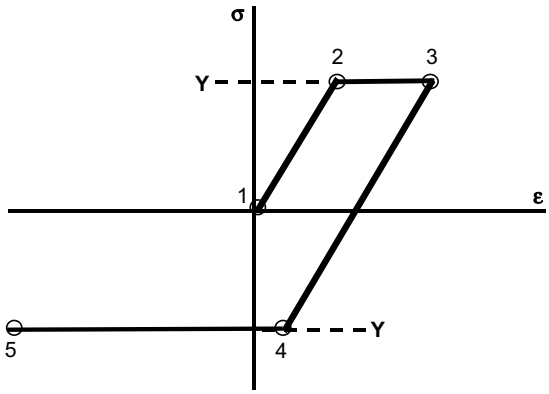

Fig. 10. Behavior of a single friction–spring element.

element yields again (point 4). Two things can be observed from this behavior. One is that, when the friction element has yielded under increasing strain, and then the strain is decreased, the friction element locks. The stiffness for decreasing strain at this point (point 3) is equal to the spring stiffness. Also, for the friction element to yield again as the strain decreases, the strain must decrease by twice the amount initially required for yielding. This allows the stress in the spring to first go to 0 before increasing in the opposite direction to the point of yielding.

The continuous yielding element can be represented as many of these friction–spring elements in parallel as shown before in Fig. 7. When the strain increases from 0, the yielded area fraction, a_y, increases with stress at a rate μ. As the strain stops increasing and starts decreasing, all the friction elements that had previously yielded, now lock. The stiffness of the system now is the initial stiffness and, hence, the yielded area fraction is 0. As the stress decreases, the yielded area fraction increases in proportion to the stress change from this point, i.e., it will be proportional to the absolute value of the difference between the current stress and the stress at the point when the elements lock. Also, as seen before in the case of a single friction–spring element, the strain in each of the infinitesimal elements of the continuously yielding element

should decrease by twice its initial yielding strain before it yields again. So, the yielded area fraction now increases from 0 at a rate [2] $\mu/2$, instead of μ, with respect to the stress. This can be expressed as follows:

$$a_y = \frac{\mu}{2}|\sigma - \sigma_{sc}| \tag{11}$$

where σ_{sc} is the stress at the sign change of the strain rate, i.e., the stress at the point when the strain stops increasing and starts decreasing or vice versa. In an incremental algorithm this can be implemented in the following way:

if $a_y > a_{y\max}$ then

$$\phi = \mu$$

$$a_{y\max} = a_y$$

else

$$\phi = \mu/2$$

where $a_{y\max}$ is the maximum area yielded in the entire history and ϕ is the rate of yielding. The corresponding stress for a given strain sequence can be calculated as shown:

$$a_y = \phi|\sigma_i - \sigma_{cos}|$$

$$k = (1 - a_y)K$$

$$d\sigma = k\,d\varepsilon$$

$$\sigma_{i+1} = \sigma_i + d\sigma$$

Fig. 11 shows the behavior of the continuously yielding element for a sinusoidal strain variation.

Consider another strain history as shown in Fig. 12. As the strain increases along the path from points 0 to 1, the rate of yielding is μ, since all the springs start from a zero stress state. Say that n_1 elements, of a large number of elements, yield in this process as shown in Fig. 13. Now as the strain decreases along the path from points 1 to 2, the rate of yielding is $\mu/2$, since the elements that previously yielded in the positive direction now yield in the negative direction. Say n_2 elements yield in this process. Since the rate of yielding along the path from points 1 to 2 does not exceed $\mu/2$, $n_2 < n_1$. As the strain decreases along the path from points 1 to 2, the friction elements of the $(n_1 - n_2)$ elements stay locked and the stresses in these elements decrease. Now, as the strain increases along the path from points 2 to 3, the rate of yielding is again $\mu/2$ and the n_2 elements that had previously yielded, yield again as the stress reaches point 3. The friction elements of the $(n_1 - n_2)$ elements stay locked and the stresses in these elements increase by the same amount. So, at point 3 all these $(n_1 - n_2)$ elements are at a point of incipient yielding and begin to yield as the strain increases beyond point 3. Hence at point 3 the yielded area fraction (a_y) has the value that it had at point 1.

This logic is implemented in an algorithm as follows: whenever the yielded area fraction at the current stress reversal is less than the yielded area fraction at the previous stress reversal, the yielded area fraction, (a_y), the stress, (σ_{sc}), and the sign of the stress rate, at the previous stress reversal are appended to arrays of such stored values. At every time step, the value of current value of stress and sign of stress rate are

[2] The rate at which a_y increases is equal to the rate at which the elements yield with stress and will sometimes be referred to as the rate of yielding.

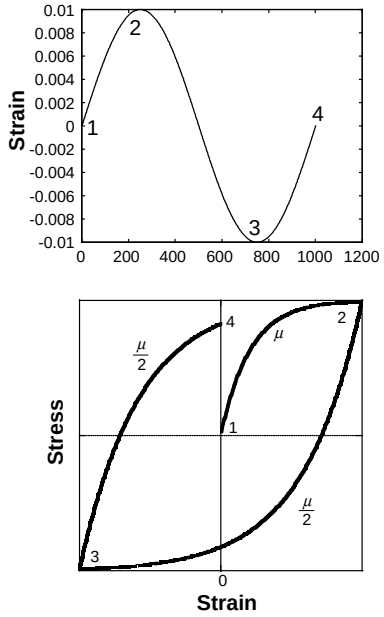

Fig. 11. The stress–strain behavior for a sinusoidal strain history.

compared to the stresses and the corresponding signs of stress rate in the arrays of stored extreme points, starting from the most recently stored values.

Whenever the current stress exceeds the stress stored in the array with the same sign of the stress rate (dir), the current yielded area is replaced by the stored yielded area. The stored arrays are then truncated, deleting the values just used and any values after it. For example, in the strain history being considered, the data of point 1 is stored at point 2 and is removed at point 3.

Thus, a continuously yielding friction element is developed which captures the effective behavior of many discrete friction–spring elements in parallel. Parameter identification and a comparison to the initial discrete model are made in the results section.

3. Linear fractional derivative model

In the NMAF model, the relaxation equations, Eq. (2), are first order in time and hence multiple internal fields (anelastic strains) are required to capture the relatively weak frequency dependence of the loss factor. By using a fractional derivative operator in the evolution equations for the anelastic strains, the observed material behavior can be accurately described using a single anelastic strain (Enelund and Lesieutre, 1998). In the fractional derivative approach, the relaxation equation takes the following form:

$$\sigma^{\mathrm{A}} = \frac{cG_u}{\Omega} D^{\alpha}(\varepsilon^{\mathrm{A}}) = G_u(\varepsilon - c\varepsilon^{\mathrm{A}}) \tag{12}$$

where D^{α} is the derivative operator of order α ($0 < \alpha < 1$) G_u is the high frequency modulus, Ω corresponds to the relaxation time at constant strain, and c is obtained from the high frequency and low frequency moduli (Eq. (13)). The above equation relates the stress in the fractional dashpot (Fig. 14), or the anelastic stress, to the anelastic strain. It also relates the anelastic stress to the total strain.

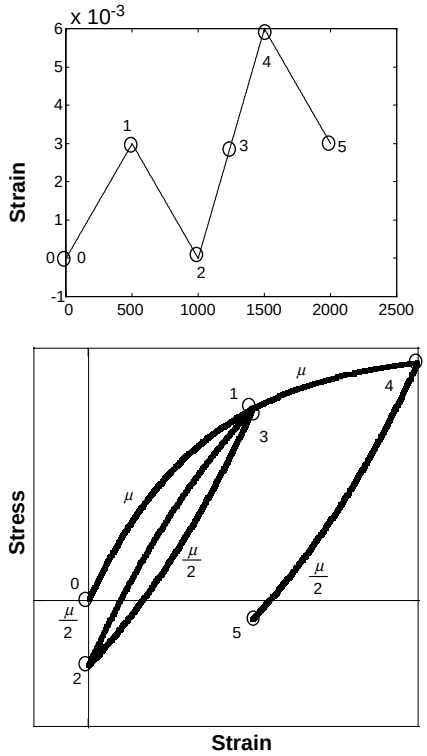

Fig. 12. Strain sequence and associated stress–strain behavior.

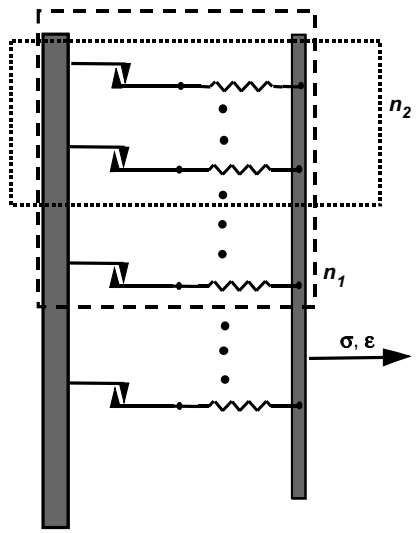

Fig. 13. Schematic to illustrate the properties of a continuously yielding element.

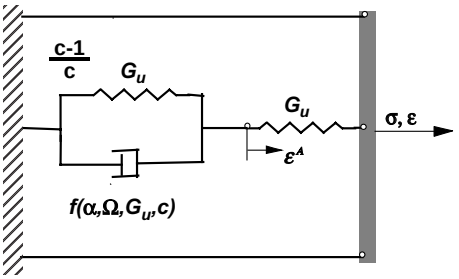

Fig. 14. Schematic of fractional derivative model.

$$c = \frac{G_u}{G_u - G_r} \tag{13}$$

The total stress can be calculated from the total strain and anelastic strain as follows:

$$\sigma = G_u(\varepsilon - \varepsilon^{\mathrm{A}}) \tag{14}$$

By applying Fourier transforms to Eqs. (12) and (14) and eliminating the anelastic strains, the corresponding dynamic modulus is obtained as

$$G(\omega) = G_u - \frac{(G_u - G_r)}{(1 + (\mathrm{i}\omega/\Omega)^{\alpha})} \tag{15}$$

where ω is the frequency, G_u is the high frequency modulus, and G_r is the low frequency modulus.

The fractional derivative model can be represented schematically as shown in Fig. 14.

3.1. Time domain modeling of the fractional ADF element

This fractional derivative model must be implemented in the time domain in order to introduce amplitude-dependent nonlinearity, i.e., time integration of the fractional derivative is required. To do this, the Grunwald definition of the fractional derivative is used, which, when discretized in time, gives (Oldham and Spanier, 1974):

$$\left(D^{\alpha}(\varepsilon^{\mathrm{A}})\right)_{n+1} = \frac{\left((\varepsilon^{\mathrm{A}})_{n+1} + \sum_{j=1}^{n} B_j(\alpha)(\varepsilon^{\mathrm{A}})_{n+1-j}\right)}{(\Delta t)^{\alpha}} \tag{16}$$

where

$$B_j(\alpha) = \frac{\Gamma(j-\alpha)}{\Gamma(-\alpha)\Gamma(j+1)} \tag{17}$$

and Γ is the gamma function. Eq. (16) is used in conjunction with Eqs. (12) and (14) to calculate the stress. As seen in Eq. (16), the fractional derivative of a function at a point in time depends on the entire past time history, unlike an integer derivative, which can be obtained quite accurately from the value of the function at a finite number of previous points. In order to obtain the fractional derivative of a function, the values of the function at points in the past are weighted by a factor B_j, which is itself a function of the time index, j, and order of differentiation, α. The variation of this factor B_j with index is illustrated in Fig. 15. As seen in Fig. 15, the value of B_j decreases with increasing index.

This implies that the value of the function at points in the past closest to the current point have more effect on the current value of the fractional derivative, and that the value of the function at points further

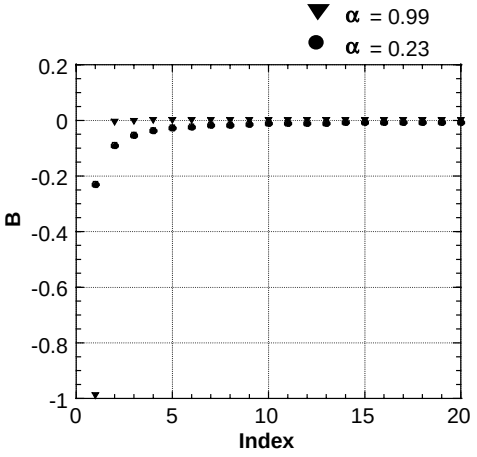

Fig. 15. Variation of B with index.

back in the history have a diminishing effect. This is known as "fading memory". Also, as seen in the figure for $\alpha = 0.23$, the history has a larger effect on the value of the fractional derivative than it does for $\alpha = 0.99$. The limit of the sum of the factors, B_j, as j tends to infinity, is found to be -1 for all values of α less than and including 1. This was observed through numerical calculations.

The entire history is generally needed to calculate the value of the fractional derivative at the current time. However, for practical numerical computations, the time history must be truncated. One approach is to neglect the history at times so far in the past that B_j is smaller than some threshold value. Experience has shown, however, that the error due to truncation can be large, for small α, even if a very small threshold value is chosen. The effect of truncation can be seen in Fig. 16. The test case consists of a strain history with strain linearly increasing from 0 to an arbitrary value, and constant thereafter. The anelastic strain is then plotted with time for a value of $\alpha = 0.23$. When the entire history is used, in the anelastic strain increases with time and reaches an equilibrium value. But if the strain history is truncated based on a cutoff value for B, this correct equilibrium anelastic and thus total, strain is not reached. This result was observed even if a very small cutoff value was chosen for B_j.

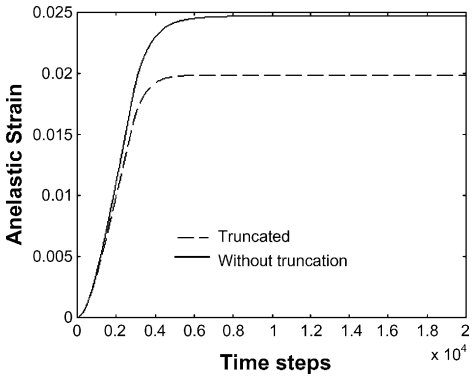

Fig. 16. Effect of truncation on the anelastic strain calculation.

The error in the calculation due to truncation is reduced by altering the values of B_j used in the calculation of the fractional derivative. The values of B_j used in the truncated calculation are multiplied by a weighting factor. Several methods of weighting were explored. One was the use of a constant value for the weight, so that the weighted sum of the truncated series of B_j, is equal to the sum of the series of B_j for a very large number of points (−1) as shown below in Eq. (18).

$$B'_j = \frac{\sum_{n=0}^{\infty} B_n}{\sum_{n=0}^{n_{\max}} B_n} B_j = -\frac{1}{\sum_{n=0}^{n_{\max}} B_n} B_j, \quad n_{\max} = \text{truncated value} \tag{18}$$

Another approach was to use an exponential weighting function so that the initial values of B_j have a larger weight than the later values as in Eq. (19).

$$B'_j = \left[1 + \left(\frac{\sum_{n=0}^{\infty} B_n}{\sum_{n=0}^{n_{\max}} B_n} - 1\right) \times \mathrm{e}^{-bj}\right] \times B_j, \quad j = 0, 1, \ldots, n_{\max} \tag{19}$$

here, however,

$$\sum_{n=0}^{n_{\max}} B'_j \neq -1 \tag{20}$$

Both these methods are very effective in correcting the relaxation behavior of the model, as seen in Fig. 17. The test case is the same as that used in Fig. 16.

The figure shows the variation of anelastic strain with time for different weighting schemes. In the figure, truncation using constant weights and truncation using exponential weights show almost the same relaxation behavior as the case in which the series of B_j was not truncated.

The anelastic displacement field model using fractional derivatives is presented both in the frequency domain and the time domain. The time domain implementation of the fractional derivative is cumbersome because it generally involves the calculation of the entire past history. The calculation time is reduced using truncation and a weighted history. A limit on the error due to truncation can also be found by a method provided by Podlubny (1999). Another way of reducing the calculations involved could be by using a sparse time history as proposed by Adolfsson et al. (2002).

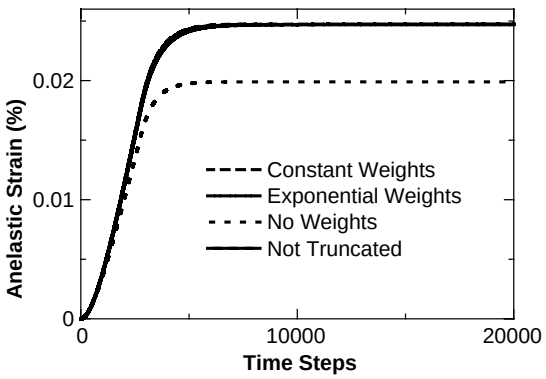

Fig. 17. Relaxation curves for different weighting schemes.

4. Nonlinearity in the fractional derivative element

In the NMAF model, a viscous nonlinearity was introduced to capture the rate-dependent amplitude dependence of the model stress–strain behavior at higher amplitudes (1–10%). This was done by introducing a cubic term in Eq. (2), the relaxation equation. The nonlinearity added makes the dashpot softer at higher amplitudes.

Several methods for introducing nonlinearity in the fractional derivative element were evaluated; four were unsatisfactory while one worked well. The first method was to introduce a nonlinear relation between the anelastic stress and fractional derivative of the anelastic strain, instead of a linear relation, as shown in Eq. (21)

$$D^{\alpha}(\varepsilon^{\mathrm{A}}) = \frac{\Omega^{\alpha}}{cG_u}(\sigma^{\mathrm{A}}) + C_2(\sigma^{\mathrm{A}})^n \tag{21}$$

In this equation, C_2 is the coefficient multiplying the nonlinear term, and n is any positive number. This method does not work well for small values of α ($\alpha < 0.5$). For small values of α, the fractional derivative at the current time depends strongly on the history, as seen previously. So, making the fractional derivative proportional to the nth power of the anelastic stress at the current time does not have much effect.

The second method that was considered involved making the strain rate proportional to the current anelastic stress and to a weighted history of the stress points, instead of to a single point in the past. This approach however, did not yield acceptable results.

The third method involved making the order of fractional differentiation amplitude dependent, and the fourth involved making the weighting functions amplitude dependent. The former did not give elliptical stress–strain loop shapes for a sinusoidal strain and the latter did not predict the loss modulus well. Both these methods, however, produced significant nonlinear behavior. The entire past history of anelastic strain was used in these methods.

Hence to introduce nonlinearity effectively, the entire history should be included in the calculation of any nonlinear behavior. Using this insight, a nonlinear term involving the anelastic stress was introduced in the history as shown in Eq. (22). This approach is similar to the one used in the NMAF model when $\alpha = 1$.

$$D^{\alpha}(\varepsilon^{\mathrm{A}}_{n+1}) = \frac{\left(\varepsilon^{\mathrm{A}}_{n+1} + \sum_{j=1}^{n} B_j(\alpha)\left(\varepsilon^{\mathrm{A}}_{n+1-j} + k_{\mathrm{nl}}\sigma^{\mathrm{A}}_{n+1-j}\left|\sigma^{\mathrm{A}}_{n+1-j}\right|\right)\right)}{(\Delta t)^{\alpha}} \tag{22}$$

This method works well with the ADF model, and model predictions look very much like the experimental data, as will be seen in the results shown later.

5. Parameter identification and comparison of the models

Initial parameters for the current model were obtained by comparing individual parts of the new model to individual parts of the NMAF model. Using the parameters so obtained as a starting point, model predictions are compared to experimental data, and the parameters are adjusted to improve agreement.

5.1. Continuously yielding element

The continuously yielding model was fit to the set of discrete friction elements of the NMAF model, the parameters of which were previously obtained by fitting to experimental data. Three discrete friction–spring pairs were used in the NMAF model, requiring six parameters. The initial stiffness K, was obtained from the discrete friction–spring elements by summing the stiffnesses of all the springs. The reciprocal of the

maximum yield stress gives the rate parameter, μ. The parameters of the discrete friction elements and the corresponding continuous yielding element are given in Table 1. Fig. 18 shows the stress strain hysteresis loops obtained from both models. The current model, with just two parameters (μ and K), captures the stress strain behavior shown by the three discrete elements quite accurately. In fact, it has a much smoother behavior than that of the three discrete friction–spring pairs, which is more typical of real material behavior.

In the continuously yielding element, the rate parameter, μ, is the reciprocal of the stress at which the element yields completely and the stiffness parameter, K, is the initial stiffness of the element. This physical insight is useful in determining parameters uniquely from data.

5.2. Linear fractional derivative element

The initial parameters of the linear fractional derivative model were estimated using the variation of storage modulus and loss factors predicted by the linear multi-ADF part of the NMAF model over a frequency range of 0.01–1000 Hz. The parameters were determined using an optimization procedure that reduced the weighted error in the complex modulus at different points in the considered range of frequencies. This range was chosen to completely capture the variation of the loss factor as predicted by the NMAF model. The results, along with the parameters of the NMAF model that were used for characterization are given in Table 2.

Table 1
Parameters used in the friction models

Discrete elements	G_i (psi)	Y_i (psi)	**Continuous yielding element**
Spring 1	194.5	0.134	$\mu = 1.35$ psi^{-1}
Spring 2	102.7	0.246	$K = 380.44$ psi
Spring 3	83.24	0.418	

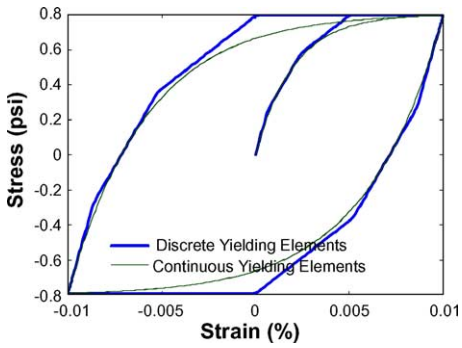

Fig. 18. Comparison of the continuous and discrete yielding elements.

Table 2
Characterization parameters and results

NMAF model $G_u = 312$ psi		**Fractional derivative model**	
$C_1 = 4.49$	$\Omega_1 = 0.05$ rad/s	$\alpha = 0.23$	$G_u = 410$ psi
$C_2 = 5.05$	$\Omega_2 = 3.25$ rad/s		
$C_3 = 3.31$	$\Omega_3 = 120.5$ rad/s	$C = 1.1197$	$\Omega = 19.3$ rad/s

5.3. Complete model—characterization

Using the parameters thus obtained as a starting point, predictions made using the entire combined model, including the nonlinearity in the fractional derivative part are, compared to experimental data. A gradient-based optimization method was used to vary the parameters to improve the fit to experimental data. This experimental data used consisted of a frequency sweep (0.01–10 Hz) at 1% strain amplitude, and an amplitude sweep from (0.1–10% strain) at 1 Hz.

The effective storage and loss moduli predicted by the model are compared to experimental data in Figs. 19 and 20. The corresponding model parameters are listed in Table 3. As seen in the figure, the predictions vary smoothly with both amplitude and frequency, and the model does a better job of capturing the material behavior with far fewer parameters than the number used in the NMAF model.

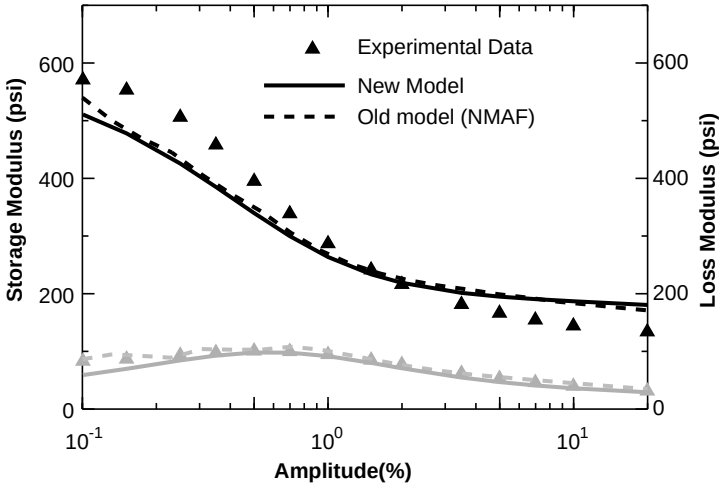

Fig. 19. Amplitude variation of complex modulus predicted by the two models compared to experimental data at 1 Hz.

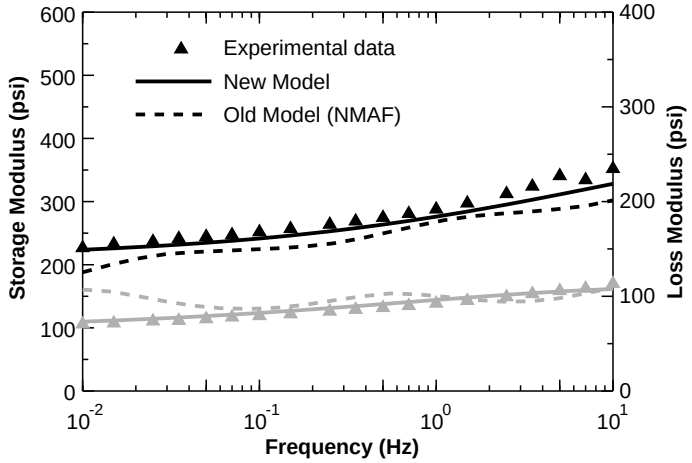

Fig. 20. Frequency variation of complex modulus predicted by the two models compared to experimental data at 1% strain amplitude.

Table 3
Characterization parameters and results

Fractional derivative model			
$\alpha = 0.365$	$G_u = 443$ psi	$k_{nl} = 9.5e{-}6$ psi^{-2} (nonlinear factor in Eq. (22))	
$C = 1.44$	$\Omega = 147$ rad/s	$K = 400$ psi	$\mu = 1.144$ psi^{-1}

5.4. Complete model—validation

To validate the model, predictions of the variation of complex modulus with frequency and amplitude are compared to experimental data that were not used in the parameter identification. Model predictions of frequency variation at 10% strain amplitude and amplitude variation at 10 Hz are compared to experimental data as shown in Figs. 21 and 22. The new model gives smoother results, more representative of real

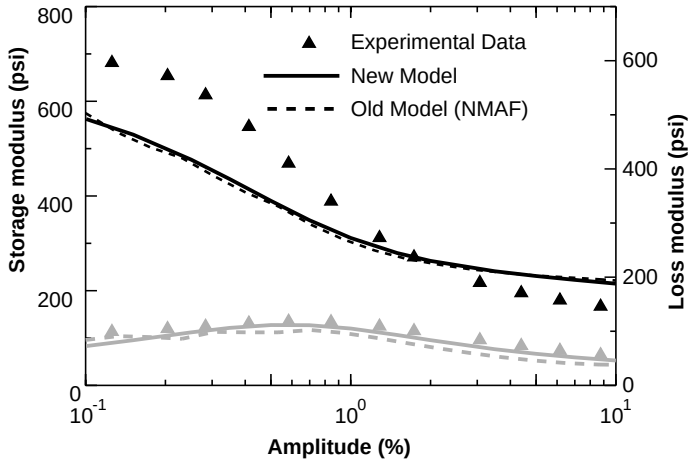

Fig. 21. Amplitude variation of complex modulus predicted by the two models compared to experimental data at 10 Hz.

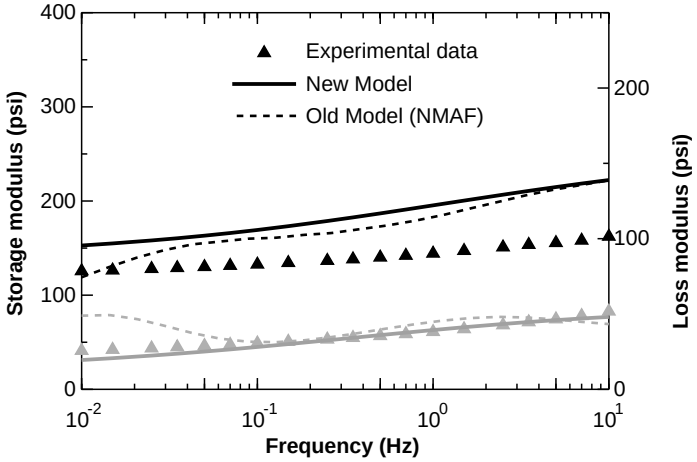

Fig. 22. Frequency variation of complex modulus predicted by the two models compared to experimental data at 10% strain amplitude.

material behavior than those of the NMAF model. The NMAF model, due to its discrete nature, has shallow inflections in its predictions.

6. Conclusion

The previously developed NMAF model describes the behavior of the elastomer in the considered range reasonably accurately, but requires 16 parameters to do so. This model uses multiple nonlinear ADF elements in parallel with multiple discrete friction–spring pairs. A new continuously yielding element, containing two parameters, was developed and used to replace the discrete friction element part (six parameters) of the NMAF model. The linear multi-ADF part (seven parameters) of the NMAF model was replaced by the fractional derivative ADF model (four parameters). Different methods of introducing nonlinearity into the element were evaluated and a nonlinear fractional derivative element was developed with the addition of two parameters. The number of parameters required to accurately capture elastomeric behavior was reduced by 9, from 16 to 7.

The different parts of the new model were integrated and its performance was compared to that of the NMAF model. The new model captures the frequency and amplitude variation of the storage and loss moduli of the material better than the NMAF model. The parameters of the new model, while fewer in number, also have better physical interpretation. The parameters of the continuously yielding element depend on the initial stiffness and ultimate yield stress of the element. The parameters of the fractional derivative element are related to the high frequency modulus, low frequency modulus, the relaxation time at constant strain and variation of loss factor with frequency. The nonlinear parameter can be obtained by examining the behavior of the model at higher amplitudes.

References

Adolfsson, K., Enelund, M., Larsson, S., 2002. Adaptive discretization of fractional order viscoelastic constitutive equations using sparse time history. In: Presented in 39th Annual Technical Meeting Society of Engineering Science, State College, PA, 13–16 October.

Austrell, P., 1997. Modeling of Elasticity and Damping for Filled Elastomers. Ph.D. Dissertation, Lund University, Lund Institute of Technology, Division of Structural Mechanics, Sweden.

Bagley, R.L., Calico, R.A., 1991. Fractional order state equations for the control of viscoelastically damped structures. Journal of Guidance, Control and Dynamics 14 (2), 304–311.

Bagley, R.L., Torvik, P.J., 1983. Fractional calculus—a different approach to viscoelastically damped structures. AIAA Journal 21 (5), 741–748.

Bagley, R.L., Torvik, P.J., 1985. Fractional calculus in the transient analysis of viscoelastically damped structures. AIAA Journal 23 (3), 201–210.

Brackbill, C.R., Lesieutre, G.A., Smith, E.C., Ruhl, L.E., 2000. Characterization and modeling of low strain amplitude and frequency dependent behavior of elastomeric damper materials. Journal of the American Helicopter Society 45 (1).

Enelund, M., Lesieutre, G.A., 1998. Time domain modeling of damping using anelastic displacement fields and fractional calculus. International Journal of Solids and Structures 36, 4447–4472.

Gandhi, F., Chopra, I., 1996. Analysis of bearingless main rotor aeroelasticity using an improved time domain nonlinear elastomeric damper model. Journal of the American Helicopter Society 41 (3).

Govindswamy, K., Smith, E.C., Lesieutre, G.A., Beale, M.R., 1995. Characterization and modeling of strain-dependent dynamic behavior of viscoelastic elastomers in simple shear. In: Proceedings of the 36th AIAA/ASME/ASCE/AHS/ASC Structures, Structural Dynamics And Materials Conference, New Orleans, LA, April.

Kunz, D.L., 1997. Influence of elastomeric lag damper modeling of the predicted dynamic response of helicopter rotor systems. AIAA Journal (February).

Lesieutre, G.A., 1992. Finite elements for dynamic modeling of uniaxial rods with frequency dependent material properties. International Journal of Solids and Structures 29 (12), 1567–1579.

Lesieutre, G.A., Bianchini, E., Maiani, A., 1996. Finite element modeling of one-dimensional viscoelastic structures using anelastic displacement fields. Journal of Guidance, Control and Dynamics. 19 (3).

Oldham, K.B., Spanier, J., 1974. The Fractional Calculus. Academic Press, New York.

Panda, B., Mychalowycz, E., Tarzanin, F.J., 1996. Application of passive dampers to modern helicopters. Journal of Smart Materials and Structures 5 (October).

Podlubny, I., 1999. Fractional Differential Calculus. Academic Press, New York.

Ramrakhyani, D.S., Lesieutre, G.A., Smith, E.C., 2001. Efficient modeling of elastomeric materials using fractional derivatives and plastic yielding. In: Proceedings of the 42nd AIAA/ASME/ASCE/AHS/ASC Structures, Structural Dynamics, and Materials Conference and Exhibit, Seattle, WA, 16–19 April 2001.

Ramrakhyani, D.S., Lesieutre, G.A., Smith, E.C., 2002. Nonlinear modeling of dynamic behavior of elastomeric materials. In: Proceedings of 43rd AIAA/ASME/ASCE/AHS/ASC Structures, Structural Dynamics, and Materials Conference and Exhibit, Denver, CO, 22–25 April 2002.